Geophysical Research Letters

RESEARCH LETTER
10.1029/2024GL112237

Changes to Atmospheric River Related Extremes Over the United States West Coast Under Anthropogenic Warming

Timothy B. Higgins[1], Aneesh C. Subramanian[1], Peter A. G. Watson[2], and Sarah Sparrow[3]

[1]Department of Atmospheric and Oceanic Sciences, University of Colorado Boulder, Boulder, CO, USA, [2]School of Geographical Sciences, University of Bristol, Bristol, UK, [3]Department of Atmospheric, Oceanic, and Planetary Physics, Oxford University, Oxford, UK

Key Points:

- Extreme Atmospheric river (AR) frequency can increase by almost one order of magnitude in mild warming scenarios relative to early 21st century forcing
- The chance of unprecedented numbers of extreme AR events in a winter season increases in climate warming scenarios
- Changes in extreme AR frequency are disproportionately large in weather regimes with historically high AR frequencies

Supporting Information:

Supporting Information may be found in the online version of this article.

Correspondence to:

T. B. Higgins,
timothy.higgins@colorado.edu

Citation:

Higgins, T. B., Subramanian, A. C., Watson, P. A. G., & Sparrow, S. (2025). Changes to atmospheric river related extremes over the United States west coast under anthropogenic warming. *Geophysical Research Letters*, *52*, e2024GL112237. https://doi.org/10.1029/2024GL112237

Received 29 AUG 2024
Accepted 19 FEB 2025

Abstract Despite advances in our understanding of changes to severe weather events due to climate change, uncertainty regarding rare extreme events persists. Atmospheric rivers (ARs), which are directly responsible for the majority of precipitation extremes on the US West Coast, are projected to intensify in a warming world. In this study, we utilize two unique large-ensemble climate models to examine rare extreme AR events under various warming scenarios. By quantifying changes to rare extremes, we can gain some insight into the potential for these destructive unprecedented events to occur in the future. Additionally, the abundance of data used in this study enables changes to both seasonal extreme AR occurrences and changes to extremes during various synoptic-scale flow patterns to be explored. From this analysis, we find substantial changes to AR extremes under even mild warming scenarios with disproportionately large changes during weather regimes that are conducive to AR activity.

Plain Language Summary Atmospheric rivers (ARs) are sources of moisture that can cause destructive flooding events on the US West Coast. Constraints on computational resources is partially responsible for our limited understanding of how extreme AR events will be impacted by future climate warming. This study uses large model simulations that were created from a unique approach to gain insight into possible changes to such events under various warming scenarios. It also examines changes to seasonal characteristics of extreme AR events and changes during various atmospheric flow patterns.

1. Introduction

Atmospheric Rivers (ARs) are elongated corridors of water vapor that are closely associated with extreme precipitation events on the US west coast (Neiman et al., 2008). While weak ARs can be beneficial by functioning as a water source in a region that is prone to drought, extreme ARs can be dangerous and damaging (Corringham et al., 2022; Ralph et al., 2019; Rhoades et al., 2021). The annual cost of damage from ARs is on the order of billions of dollars (Corringham et al., 2019). In 2017, a single crisis worsened by AR activity at the Oroville dam cost roughly 1 billion dollars in infrastructure repairs (Henn et al., 2020). Future climate projections show increases in AR precipitation and decreases in non-AR precipitation (Gershunov et al., 2019).

The number of AR days in CMIP5 projections under the RCP 8.5 scenario is expected to roughly double in the midlatitudes over the North Pacific during winter months, with thermodynamic changes dominating and dynamic changes having no significant effect (Gao et al., 2015). Michaelis et al. (2022) simulated an extreme AR event that occurred in 2017 with perturbations to reflect four different climate change scenarios and found that the thermodynamic component enhanced AR moisture by a 10% integrated vapor transport (IVT) increase per °C and changes to AR wind speed accounted for a 4% IVT increase per °C. ARs are projected to increase in length and width while occurring more frequently in the midlatitudes (Espinoza et al., 2018; O'Brien et al., 2022) and the peak season of AR flooding hazards is projected to increase in length (Dettinger, 2011). Understanding the degree to which extreme AR events and seasonal AR extremes change in the future is critical for the long-term planning of adaptation strategies to climate change. By quantifying these changes with high-resolution large ensemble simulations, this study will provide a unique new insight into the future of extreme AR events, which was not possible previously due to the lack of available high-resolution large ensemble climate model runs.

The uncertainty of AR frequency trends across AR detection methods far exceeds the uncertainty across climate models (Shields et al., 2023). However, ARs with high intensities have lower detection uncertainty (Rutz et al., 2019). In this study, we quantify the impacts of anthropogenic forcing on extreme ARs in large ensemble

simulations of both the Hadley Centre Atmospheric Model version 4 (HadAM4) (Bevacqua et al., 2021; Leach et al., 2022) and the Community Earth System Model version 2 (CESM2) large ensemble (Rodgers et al., 2021). The abundance of data enables robust calculations of changes to AR extremes in these models, which are defined by absolute thresholds of maximum AR IWV occurring at a frequency of less than once per year on average derived from the early 21st century climate in this study. After quantifying changes to future individual events overall, we further examine the changes under varying weather regimes.

Weather regimes are described as a limited number of recurrent and quasi-stationary intraseasonal large-scale patterns in the atmosphere that are interrupted by transition periods (Kimoto & Ghil, 1993; Vautard, 1990). Regimes over the North Pacific can be predicted in the subseasonal to seasonal (S2S) range, which is considered to be 2 weeks to several months into the future (Vitart et al., 2017). They can be indicators of regional vulnerability to future flooding events caused by ARs (DeFlorio et al., 2019; Higgins et al., 2024). Varying weather regimes can have different levels of predictability, which can influence the amount of damage that extreme events cause. Changes to rare extreme AR events are assessed during each weather regime to better understand possible synoptic-scale dynamical shifts of extreme activity. Changes to extreme AR activity under varying weather regimes were only assessed in HadAM4 data to ensure an adequate sample size in every regime.

2. Data and Methods

2.1. Model Simulations

The citizen-science project, climateprediction.net (CPDN), was used to generate a large ensemble data set by running the HadAM4 global atmosphere and land surface model (Williams et al., 2003). With the assistance of computing power from volunteers' computers, three warming scenarios with at least 1,800 winter (December–February) simulations were generated (Bevacqua et al., 2021). The horizontal grid resolution is 0.83° × 0.56°, which is finer than that of most model outputs from CMIP5 and CMIP6, and the temporal resolution output is 6 hr. This model simulates western North American atmospheric dynamics and precipitation with comparable quality to other state-of-the-art CMIP models but is more computationally efficient and can be run on personal computers, allowing very large ensembles to be produced.

The simulations were produced following the Half a degree Additional warming, Prognosis, and Projected Impacts (HAPPI) framework, which employs prescribed fields of sea surface temperature, sea ice concentration, greenhouse gases, and aerosols (Mitchell et al., 2017). The historical scenario (2,889 members) uses forcing from 2006 to 2015 (close to 1°C warmer than preindustrial levels) and the warming scenarios impose SST perturbations corresponding to global warming stabilization scenarios at 1.5°C (2,006 members) and 2°C (1,882 members) warmer than preindustrial levels. Clausius-Clapeyron scaling was estimated from regional SST changes. Every year that was used for forcing accounted for 9%–11% of ensemble members from each scenario. The HAPPI framework uses weighted RCP scenarios in CMIP5 model runs to provide boundary conditions for the given global warming levels. The simulations were initialized on 1 November of each winter, with initial condition perturbations applied to generate an ensemble in each year of each scenario, with the entire month of November discarded as spinup.

The CESM2 Large Ensemble is an open-source global coupled climate model comprising ocean, atmosphere, land surface, sea ice, land ice, and wave models (Danabasoglu et al., 2020). It has various changes from its previous version (CESM1), including a unified turbulence scheme and an updated cloud physics scheme. This study considers a historical scenario with forcing from 2007 to 2014 and the SSP 3-7.0 forcing scenario (4°C increase relative to preindustrial levels at the end of the century) with smoothed biomass burning during the years 2092–2099 are considered. This warming scenario is far more severe than the previously mentioned HAPPI scenarios. The historical scenario and the SSP 3-7.0 scenario output 40 and 50 ensemble members, respectively that include the variables used to track ARs. Therefore, this study analyzes 320 winter seasons in the historical scenario and 400 winter seasons from the SSP 3-7.0 scenario in CESM2. The considerably lower sample size of CESM2 relative to the HadAM4 simulations only enabled an analysis of overall occurrences and was not sufficient for understanding changes to events under varying weather regimes. The horizontal grid resolution is 1.25° × 0.94°, and the temporal output is 6 hr. IWV, mean sea level pressure (MSLP), zonal wind velocity at 850 mb, and meridional wind velocity output were used from the output of both CESM2 and HadAM4.

2.2. AR Detection

The computational restrictions on model output and data storage of HadAM4 simulations created several obstacles for AR detection. Data from the batches that were used were only stored in the northern hemisphere, which only allowed a regional spatial domain to be used. IVT, which is often a required input field for AR detection methods, was not available in the data output. Processing the amount of data used in the study is also a highly computationally expensive task that requires the use of an efficient AR detection method. To address all of these challenges, CG-Climate (Higgins et al., 2023) was used to track ARs to address all of these challenges.

CG-Climate uses a lightweight convolutional neural network, CGNet (Wu et al., 2019) to track ARs. It can run at a high speed with high computational efficiency and is flexible with varying spatial domains. It also requires IWV as an input field instead of IVT, making it compatible with HadAM4 output. In addition to IWV, MSLP and 850 mb wind velocity were used for detection. CG-Climate uses the human expert hand-labeled data set, ClimateNet (Kashinath et al., 2021), for training. AR detection methods often exhibit high variability amongst themselves (Inda-Díaz et al., 2021), with some being more permissive than others. When CG-Climate was compared to methods from the AR Tracking Methods Intercomparison Project (ARTMIP) (Shields et al., 2018), there was little bias in the frequency of events and strong consistency in detecting the same events as other methods, but the horizontal extent of the ARs was typically larger (Higgins et al., 2023).

2.3. AR Extremes

Uncertainties that result from AR detection can have a significant impact on the shape and size, which can lead to inconsistencies between studies that use different detection methods. Only AR extremes are analyzed (Rutz et al., 2019) to avoid this issue. The intensity of ARs is calculated by taking the maximum IWV magnitude intersecting with the coastline and existing within an AR event. AR masks are connected temporally to avoid single AR events disproportionately contributing to frequency statistics. Extreme AR events are defined as AR events with intensities that meet a threshold of IWV and precipitation that occurs less than once per year on average in the historical scenarios (i.e., 32.98 mm of IWV in HadAM4 and 32.34 mm of IWV in CESM2 over the entire coast). This relative threshold is used to help account for model differences when comparing extreme events.

2.4. Circulation Regimes

To calculate weather regimes, we employ MiniSom (https://github.com/JustGlowing/minisom), a version of self-organizing maps (SOMs). SOMs are unsupervised neural networks that map high-dimensional data onto a lower-dimensional grid while preserving topological relationships. Here, the SOM is trained on normalized MSLP fields from HadAM4. The SOM iteratively adjusts its neurons, aligning them with input MSLP fields so that similar patterns cluster together, forming distinct weather regimes. Climatology from the HadAM4 historical scenario is used for normalization, and a 5-day running mean filter removes high-frequency variability before training. The trained SOM then classifies each time step into one of the learned regimes.

3. Results

3.1. AR IWV Event Extremes

The magnitude of extreme AR events increased in both models under all warming scenarios on the coast of both California and the Pacific. Differences between magnitudes of extreme events in the historical and warming scenarios from HadAM4 remained relatively consistent at all frequencies. Changes to extremes from the historical to the 2°C increase scenario were significant at the 95% level when bootstrapping was used to calculate confidence intervals for return periods of 1, 10, and 100 years (Table 1). In California, the maximum AR IWV percentage increase from the historical scenario to the 2°C increase scenario (1°C SST difference) was 13% for 1-year events, 10% for 10-year events, and 9% for 100-year events. The result was not consistent with the Clausius Clapeyron relation because the difference was larger than 7% per °C of warming. For some of the most extreme events, there was almost an order of magnitude increase in frequency when events from the historical scenario were compared to events in the 2°C warming scenario (e.g., a 100-year event in the historical scenario occurred almost once every 10 years in the 2°C increase scenario in California) (Table 1).

Table 1
Ninety-Five Percent Confidence Intervals of Extreme Atmospheric Rivers at Return Periods of 1, 10, and 100 years

California	1 year	10 years	100 years
HadAM4 HIST	31.49–32.08	40.70–41.36	45.80–47.41
HadAM4 1.5°C	34.37–34.96	43.53–44.46	48.03–49.39
HadAM4 2°C	35.59–36.27	44.55–45.67	49.35–52.19
CESM2 HIST	31.56–32.86	39.90–41.53	44.74–49.36
CESM2 SSP 3-7.0	39.33–40.75	51.21–53.64	57.16–61.63
Pacific Northwest	**1 year**	**10 years**	**100 years**
HadAM4 HIST	24.76–25.52	34.68–35.28	39.80–40.91
HadAM4 1.5°C	27.10–27.91	36.42–37.15	40.76–42.50
HadAM4 2°C	28.44–29.21	38.11–38.95	42.95–44.55
CESM2 HIST	26.55–27.38	32.81–33.81	35.04–39.14
CESM2 SSP 3-7.0	32.03–32.93	41.43–43.08	46.18–48.33

Note. Bootstrapping was used to calculate 95% confidence intervals.

Under the SSP 3-7.0 warming scenario in CESM2, IWV events that occur once every 100 years in the historical scenario happen roughly once every 2–3 years when threshold-free machine learning detection was applied. The gap between IWV extremes in the historical scenario and the SSP 3-7.0 scenario (2.5°C SST difference) was greater than a 7% per degree increase at all frequencies, suggesting that changes to AR extremes in CESM2 are also greater than Clausius-Clapeyron scaling. In California, the maximum AR IWV percentage increase from the historical scenario to the SSP 3-7.0 scenario was 24% for 1-year events, 29% for 10-year events, and 26% for 100-year events. This scaling equates to 9%–11% per °C increase, which is similar to the scaling of extremes from HadAM4 simulations.

3.2. AR IWV Seasonal Extremes

Multiple extreme AR events occurring in the same season can cause large amounts of destruction within short periods (DeFlorio et al., 2024). Anthropogenic forcing has an impact on the number of extreme AR events occurring in each season (Figure 1). In all warming scenarios in both CESM2 and HadAM4, there is a decrease in the percentage of winters in which no extreme ARs occur and a notable rise in the proportion of winters experiencing at least two extreme AR events impacting both California and the Pacific Northwest. The most significant annual variations in AR extremes are observed in the CESM2 SSP 3-7.0 warming scenario. Overall, the results indicate that anthropogenic warming increases the chance of an unprecedented season of a high number of AR extremes on the US west coast.

3.3. AR Extremes During Weather Regimes

The large ensemble size of HadAM4 enabled an analysis of changes to extreme AR activity under five different weather regimes of MSLP anomalies over the North Pacific (Figure 2). Under both the 1.5°C and 2°C warming scenarios, there was minimal change from the historical scenario in the frequency of any regime. The regime with the largest change in frequency was regime 3, which increased from 17.9% to 19.54% of the data. There were also little to no changes in MSLP in either of the warming scenarios (less than 2 millibars in all locations within all regimes). The frequencies of extreme AR events increased when the 2°C increase scenario was compared to the historical scenario in the HadAM4 data set (Figure 3). For reference, the climatology of AR extremes is shown in Figure S1 in Supporting Information S1. Regimes 2, 3, and 5 had the largest overall increases in extreme event frequencies, while Regimes 1 and 4 experienced minimal increases overall to extreme events. Much of the raw

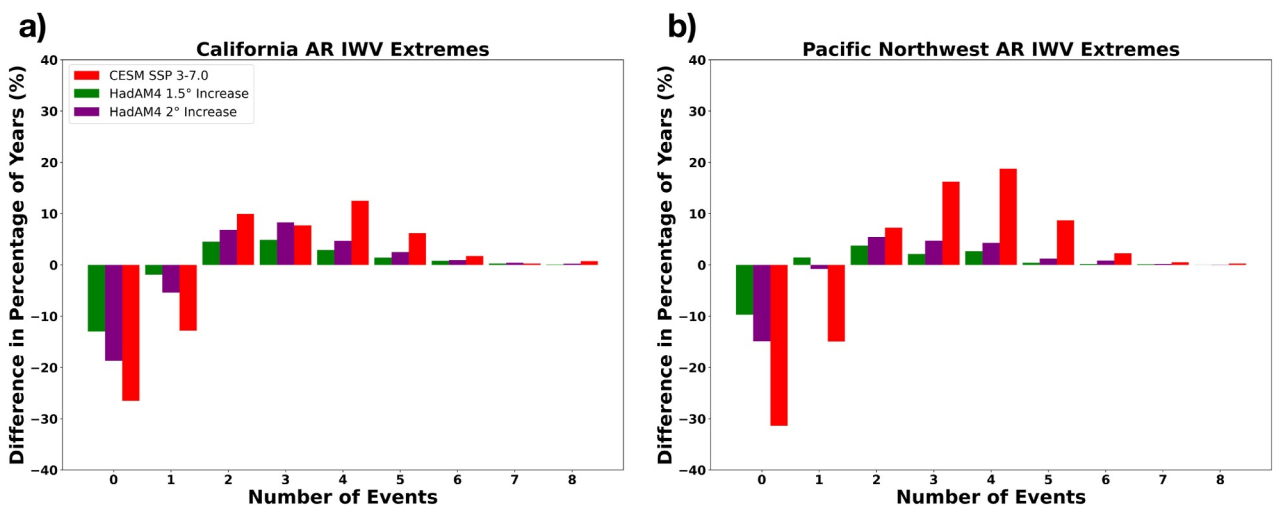

Figure 1. Change in percentage of winter seasons with particular numbers of extreme Atmospheric river (AR) events between the historical scenarios in each model and warming scenarios for extreme AR events defined by (a) California IWV and (b) Pacific Northwest IWV.

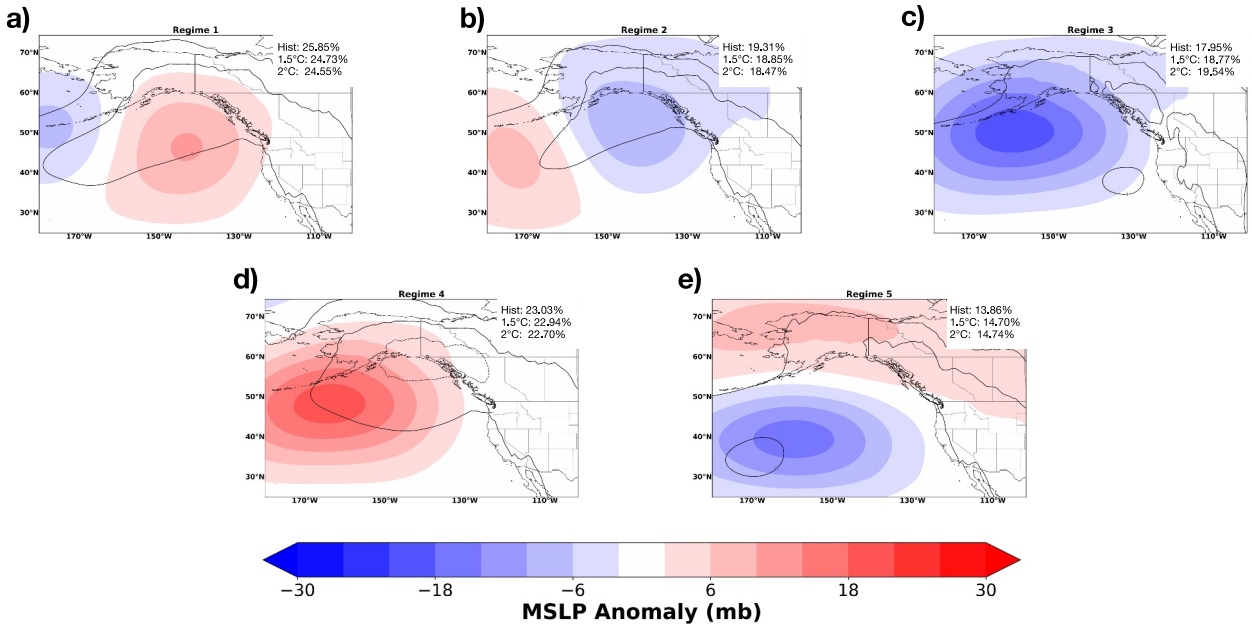

Figure 2. Winter weather regimes (a–e) from HadAM4 mean sea level pressure (MSLP) anomalies identified using the MiniSOM algorithm. MSLP anomalies across all scenarios during each regime are shown in shaded contours with increments of 4 mb. The change in MSLP anomaly from the historical scenario to the 2°C increase scenario is shown in unshaded contours with increments of 1 mb. The percentages in each panel represent the percentage of the data in each scenario that each regime falls into.

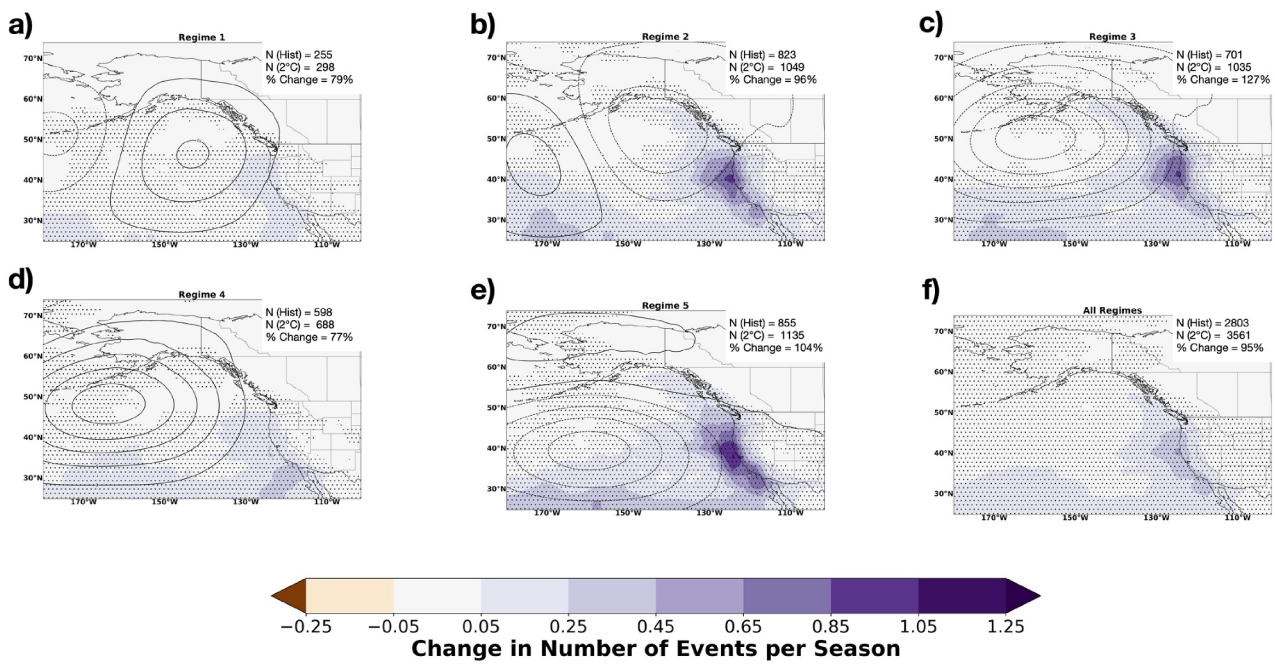

Figure 3. Changes in frequencies of extreme Atmospheric river (AR) events under each winter weather regime (a–e, filled contours, with increments of 0.25 events per year) and mean for all regimes (f). Mean sea level pressure anomalies during each weather regime are shown in line contours with increments of 6 mb. The number of detected events in each scenario and the percentage change in the number of events per season is shown in the corner of each panel. Dotted areas represent locations in which the difference between the number of extreme AR events is statistically significant at the 95% level using bootstrapping.

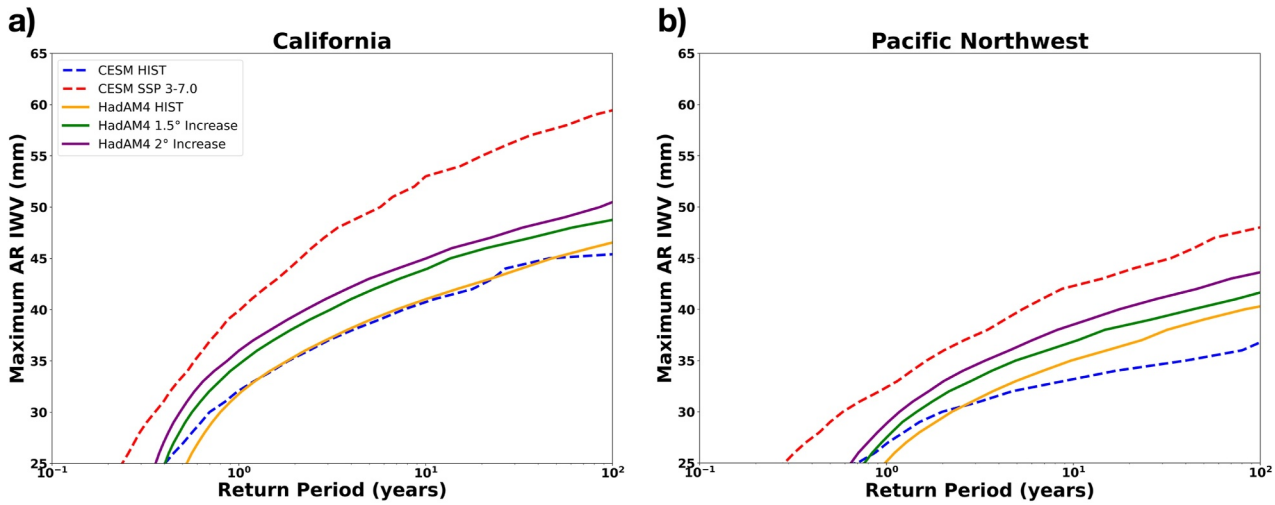

Figure 4. Maximum winter severity of (a) Pacific Northwest IWV and (b) California IWV occurring within Atmospheric river events at varying periods. The solid lines represent simulations from HadAM4, and the dashed lines represent simulations from Community Earth System Model version 2 (CESM2). The HIST scenario in HadAM4 represents historical forcing from 2006 to 2015 and the 1.5°C and 2°C scenarios represent model runs from the same years with temperature differences based on the Half a degree Additional warming, Prognosis, and Projected Impacts framework. The HIST scenario in CESM2 represents historical forcing from 2007 to 2014 and the SSP 3-7.0 scenario represents possible future forcing from 2092 to 2099.

changes in frequency can be accounted for by differences in extreme AR climatology across all regimes. However, percentage changes to extreme AR frequencies also varied under different regimes. Regimes 2, 3, and 5 also had the largest percentage changes to extreme AR frequencies (96%, 127%, and 104%, respectively) while Regimes 1 and 4 had the smallest percentage changes (79% and 77%, respectively).

The regimes with the largest increases in both raw extreme AR frequency and percentage change in extreme AR frequency (Regimes 2, 3, and 5) all have anomalously low MSLP on and near the west coast. Low pressure near the coast is often associated with moisture in southern latitudes to be transported toward the north. Figure 2 demonstrated that the magnitude of mean pressure anomalies in each regime barely changed under the global warming scenario, indicating that strengthening low pressure systems was likely not the cause of increased extreme AR frequency during these three regimes. Changes to 850 mb wind speed are also minimal (Figure S2 in Supporting Information S1). The differences are therefore unlikely to be driven by changes to synoptic-scale pressure regimes. An increase in the raw amount of moisture in southern latitudes relative to northern latitudes can impact the number of landfalling extreme ARs more during regimes that are associated with circulation patterns that facilitate poleward transport of moisture from areas near and within the tropics. This effect could drive disproportionate increases in extreme AR activity during regimes that facilitate poleward vapor transport as shown in Figure 3.

4. Discussion and Concluding Remarks

This study quantified and evaluated changes to rare AR IWV extremes in various warming scenarios. Increases in the frequency of extreme ARs along the US west coast were consistent in all warming scenarios, sometimes reaching close to an order of magnitude in the most conservative scenarios. The scaling of changes to extremes with temperature was similar in both models and greater than Clausius-Clapeyron scaling. Deviations of extreme precipitation and moisture scaling from Clausius-Clapeyron are commonly found in previous studies (Haerter & Berg, 2009; Lau & Wu, 2011; Moseley et al., 2016) and can often be related to convective feedback, including the self-organization of convective events into larger clusters. Such processes occur at the sub-grid scale and could not be analyzed with the data sets used in this study. Another possible factor in the deviation from the Clausius-Clapeyron relation is the relatively larger scaling factor that often occurs at higher altitudes, which is noted by Payne et al. (2020). The intense moisture that extreme ARs can bring at high elevations can therefore influence overall scaling. Gao et al. (2015) hypothesizes that discrepancies could also be attributed to ARs drawing from multiple pathways, with relatively more warming in the western Pacific resulting in higher overall scaling. There were also decreases in the percentage of winters with zero extreme ARs and increases in the percentage of winters with two or more extreme ARs. Differences to both individual AR extremes (Figure 4) and the number of AR

extremes in a winter (Figure 1) from the early 21st century simulations increased when the severity of the warming scenarios was increased.

Changes to weather regimes and associated AR extremes were also examined under several warming scenarios in the large ensembles from the HadAM4 model. Regime frequencies remained roughly the same across warming scenarios. The largest change in regime frequency (1.5% difference) was an increase in a regime characterized by anomalously low sea level pressure over the northeastern Pacific (Regime 3). This was the most active regime for extreme ARs to occur, potentially resulting from an extension of the North Pacific jet stream aiding the transport of water vapor toward the west coast (Neelin et al., 2013). Regimes with the most frequent AR extremes in the historical simulations also experienced the largest percentage increases in extreme AR frequency during the 2°C warming scenario. The projected changes to AR extremes resulting from rising global temperatures redefine the potential of destructive events that will realistically occur on the US west coast in the future.

Data Availability Statement

Data that can be used to re-create the figures can be accessed from Higgins (2024a). Code to create the figures can be found at Higgins (2024b).

Acknowledgments
This work is supported by the California Department of Water Resources Ph3 Atmospheric River Research Program (Award 4600014294) and the Forecast Informed Reservoir Operations Award (USACE W912HZ1920023). We would also like to acknowledge NSF NCAR HPC systems managed by CISL for providing resources that were required for many of the computations in this work. Sarah Sparrow acknowledges support from NERC (DOCILE, NE/P002099/1). We would like to thank Andrew Bowery and David Wallom at the Oxford e-Research Centre, Engineering Sciences, University of Oxford for their technical expertise. The authors acknowledge William Ingram and Simon Wilson for their support in developing HadAM4 on climatepredicitons.net (CPDN). We would like to thank both JASMIN (and CEDA) for providing the facilities required to work with (and store) CPDN large ensemble output of this scale. Finally, we would like to thank all of the volunteers who have donated their computing time to CPDN.

References

Bevacqua, E., Shepherd, T. G., Watson, P. A. G., Sparrow, S., Wallom, D., & Mitchell, D. (2021). Larger spatial footprint of wintertime total precipitation extremes in a warmer climate. *Geophysical Research Letters*, *48*(8), e2020GL091990. https://doi.org/10.1029/2020GL091990

Corringham, T. W., McCarthy, J., Shulgina, T., Gershunov, A., Cayan, D. R., & Ralph, F. M. (2022). Climate change contributions to future atmospheric river flood damages in the western United States. *Scientific Reports*, *12*(1), 13747. https://doi.org/10.1038/s41598-022-15474-2

Corringham, T. W., Ralph, F. M., Gershunov, A., Cayan, D. R., & Talbot, C. A. (2019). Atmospheric rivers drive flood damages in the western United States. *Science Advances*, *5*(12), eaax4631. https://doi.org/10.1126/sciadv.aax4631

Danabasoglu, G., Lamarque, J., Bacmeister, J., Bailey, D. A., DuVivier, A. K., Edwards, J., et al. (2020). The community Earth system model version 2 (CESM2). *Journal of Advances in Modeling Earth Systems*, *12*(2), e2019MS001916. https://doi.org/10.1029/2019MS001916

DeFlorio, M. J., Sengupta, A., Castellano, C. M., Wang, J., Zhang, Z., Gershunov, A., et al. (2024). From California's extreme drought to major flooding: Evaluating and synthesizing experimental seasonal and subseasonal forecasts of landfalling atmospheric rivers and extreme precipitation during winter 2022/23. *Bulletin of the American Meteorological Society*, *105*(1), E84–E104. https://doi.org/10.1175/BAMS-D-22-0208.1

DeFlorio, M. J., Waliser, D. E., Ralph, F. M., Guan, B., Goodman, A., Gibson, P. B., et al. (2019). Experimental subseasonal-to-seasonal (S2S) forecasting of atmospheric rivers over the western United States. *Journal of Geophysical Research: Atmospheres*, *124*(21), 11242–11265. https://doi.org/10.1029/2019JD031200

Dettinger, M. (2011). Climate change, atmospheric rivers, and floods in California - A multimodel analysis of storm frequency and magnitude Changes[1]. *JAWRA Journal of the American Water Resources Association*, *47*(3), 514–523. https://doi.org/10.1111/j.1752-1688.2011.00546.x

Espinoza, V., Waliser, D. E., Guan, B., Lavers, D. A., & Ralph, F. M. (2018). Global analysis of climate change projection effects on atmospheric rivers. *Geophysical Research Letters*, *45*(9), 4299–4308. https://doi.org/10.1029/2017GL076968

Gao, Y., Lu, J., Leung, L. R., Yang, Q., Hagos, S., & Qian, Y. (2015). Dynamical and thermodynamical modulations on future changes of landfalling atmospheric rivers over western North America. *Geophysical Research Letters*, *42*(17), 7179–7186. https://doi.org/10.1002/2015GL065435

Gershunov, A., Shulgina, T., Clemesha, R. E. S., Guirguis, K., Pierce, D. W., Dettinger, M. D., et al. (2019). Precipitation regime change in western North America: The role of atmospheric rivers. *Scientific Reports*, *9*(1), 9944. https://doi.org/10.1038/s41598-019-46169-w

Haerter, J. O., & Berg, P. (2009). Unexpected rise in extreme precipitation caused by a shift in rain type? *Nature Geoscience*, *2*(6), 372–373. https://doi.org/10.1038/ngeo523

Henn, B., Musselman, K. N., Lestak, L., Ralph, F. M., & Molotch, N. P. (2020). Extreme runoff generation from Atmospheric River driven snowmelt during the 2017 Oroville dam spillways incident. *Geophysical Research Letters*, *47*(14), e2020GL088189. https://doi.org/10.1029/2020GL088189

Higgins, T. B. (2024a). Changes to atmospheric river related extremes over the United States west coast under anthropogenic warming [Dataset]. *Zenodo*. https://doi.org/10.5281/zenodo.13380780

Higgins, T. B. (2024b). Changes to atmospheric river related extremes over the United States west coast under anthropogenic warming [Software]. *Zenodo*. https://doi.org/10.5281/zenodo.14533246

Higgins, T. B., Subramanian, A. C., Chapman, W. E., Lavers, D. A., & Winters, A. C. (2024). Subseasonal potential predictability of horizontal water vapor transport and precipitation extremes in the North Pacific. *Weather and Forecasting*, *39*(6), 833–846. https://doi.org/10.1175/WAF-D-23-0170.1

Higgins, T. B., Subramanian, A. C., Graubner, A., Kapp-Schwoerer, L., Watson, P. A. G., Sparrow, S., et al. (2023). Using deep learning for an analysis of atmospheric rivers in a high-resolution large ensemble climate data set. *Journal of Advances in Modeling Earth Systems*, *15*(4), e2022MS003495. https://doi.org/10.1029/2022MS003495

Inda-Díaz, H. A., O'Brien, T. A., Zhou, Y., & Collins, W. D. (2021). Constraining and characterizing the size of atmospheric rivers: A perspective independent from the detection algorithm. *Journal of Geophysical Research: Atmospheres*, *126*(16), e2020JD033746. https://doi.org/10.1029/2020JD033746

Kashinath, K., Kashinath, K., Mudigonda, M., Kim, S., Kapp-Schwoerer, L., Graubner, A., et al. (2021). ClimateNet: An expert-labeled open dataset and deep learning architecture for enabling high-precision analyses of extreme weather. *Geoscientific Model Development*, *14*(1), 107–124. https://doi.org/10.5194/gmd-14-107-2021

Kimoto, M., & Ghil, M. (1993). Multiple flow regimes in the northern hemisphere winter. Part I: Methodology and hemispheric regimes. *Journal of the Atmospheric Sciences*, *50*(16), 2625–2644. https://doi.org/10.1175/1520-0469(1993)050⟨2625:MFRITN⟩2.0.CO;2

Lau, K.-M., & Wu, H.-T. (2011). Climatology and changes in tropical oceanic rainfall characteristics inferred from Tropical Rainfall Measuring Mission (TRMM) data (1998–2009). *Journal of Geophysical Research*, *116*(D17), D17111. https://doi.org/10.1029/2011JD015827

Leach, N. J., Watson, P. A., Sparrow, S. N., Wallom, D. C., & Sexton, D. M. (2022). Generating samples of extreme winters to support climate adaptation. *Weather and Climate Extremes*, *36*, 100419. https://doi.org/10.1016/j.wace.2022.100419

Michaelis, A. C., Gershunov, A., Weyant, A., Fish, M. A., Shulgina, T., & Ralph, F. M. (2022). Atmospheric river precipitation enhanced by climate change: A case study of the storm that contributed to California's Oroville dam crisis. *Earth's Future*, *10*(3), e2021EF002537. https://doi.org/10.1029/2021EF002537

Mitchell, D., AchutaRao, K., Allen, M., Bethke, I., Beyerle, U., Ciavarella, A., et al. (2017). Half a degree additional warming, prognosis and projected impacts (HAPPI): Background and experimental design. *Geoscientific Model Development*, *10*(2), 571–583. https://doi.org/10.5194/gmd-10-571-2017

Moseley, C., Hohenegger, C., Berg, P., & Haerter, J. O. (2016). Intensification of convective extremes driven by cloud–cloud interaction. *Nature Geoscience*, *9*(10), 748–752. https://doi.org/10.1038/ngeo2789

Neelin, J. D., Langenbrunner, B., Meyerson, J. E., Hall, A., & Berg, N. (2013). California winter precipitation change under global warming in the coupled model Intercomparison project phase 5 ensemble. *Journal of Climate*, *26*(17), 6238–6256. https://doi.org/10.1175/JCLI-D-12-00514.1

Neiman, P. J., Ralph, F. M., Wick, G. A., Kuo, Y.-H., Wee, T.-K., Ma, Z., et al. (2008). Diagnosis of an intense atmospheric river impacting the Pacific Northwest: Storm summary and offshore vertical structure observed with COSMIC satellite retrievals. *Monthly Weather Review*, *136*(11), 4398–4420. https://doi.org/10.1175/2008MWR2550.1

O'Brien, T. A., Wehner, M. F., Payne, A. E., Shields, C. A., Rutz, J. J., Leung, L., et al. (2022). Increases in future AR count and size: Overview of the ARTMIP tier 2 CMIP5/6 experiment. *Journal of Geophysical Research: Atmospheres*, *127*(6), e2021JD036013. https://doi.org/10.1029/2021JD036013

Payne, A. E., Demory, M.-E., Leung, L. R., Ramos, A. M., Shields, C. A., Rutz, J. J., et al. (2020). Responses and impacts of atmospheric rivers to climate change. *Nature Reviews Earth & Environment*, *1*(3), 143–157. https://doi.org/10.1038/s43017-020-0030-5

Ralph, F. M., Rutz, J. J., Cordeira, J. M., Dettinger, M., Anderson, M., Reynolds, D., et al. (2019). A scale to characterize the strength and impacts of atmospheric rivers. *Bulletin of the American Meteorological Society*, *100*(2), 269–289. https://doi.org/10.1175/BAMS-D-18-0023.1

Rhoades, A. M., Risser, M. D., Stone, D. A., Wehner, M. F., & Jones, A. D. (2021). Implications of warming on western United States landfalling atmospheric rivers and their flood damages. *Weather and Climate Extremes*, *32*, 100326. https://doi.org/10.1016/j.wace.2021.100326

Rodgers, K. B., Lee, S.-S., Rosenbloom, N., Timmermann, A., Danabasoglu, G., Deser, C., et al. (2021). Ubiquity of human-induced changes in climate variability. *Earth System Dynamics*, *12*(4), 1393–1411. https://doi.org/10.5194/esd-12-1393-2021

Rutz, J. J., Shields, C. A., Lora, J. M., Payne, A. E., Guan, B., Ullrich, P., et al. (2019). The atmospheric river tracking method Intercomparison project (ARTMIP): Quantifying uncertainties in atmospheric river climatology. *Journal of Geophysical Research: Atmospheres*, *124*(24), 13777–13802. https://doi.org/10.1029/2019JD030936

Shields, C. A., Payne, A. E., Shearer, E. J., Wehner, M. F., O'Brien, T. A., Rutz, J. J., et al. (2023). Future atmospheric rivers and impacts on precipitation: Overview of the ARTMIP tier 2 high-resolution global warming experiment. *Geophysical Research Letters*, *50*(6), e2022GL102091. https://doi.org/10.1029/2022GL102091

Shields, C. A., Rutz, J. J., Leung, L.-Y., Ralph, F. M., Wehner, M., Kawzenuk, B., et al. (2018). Atmospheric river tracking method intercomparison project (ARTMIP): Project goals and experimental design. *Geoscientific Model Development*, *11*(6), 2455–2474. https://doi.org/10.5194/gmd-11-2455-2018

Vautard, R. (1990). Multiple weather regimes over the North Atlantic: Analysis of precursors and successors. *Monthly Weather Review*, *118*(10), 2056–2081. https://doi.org/10.1175/1520-0493(1990)118⟨2056:MWROTN⟩2.0.CO;2

Vitart, F., Ardilouze, C., Bonet, A., Brookshaw, A., Chen, M., Codorean, C., et al. (2017). The subseasonal to seasonal (S2S) prediction project database. *Bulletin of the American Meteorological Society*, *98*(1), 163–173. https://doi.org/10.1175/BAMS-D-16-0017.1

Williams, K. D., Ringer, M. A., & Senior, C. A. (2003). Evaluating the cloud response to climate change and current climate variability. *Climate Dynamics*, *20*(7–8), 705–721. https://doi.org/10.1007/s00382-002-0303-3

Wu, T., Tang, S., Zhang, R., & Zhang, Y. (2019). CGNet: A light-weight context guided network for semantic segmentation. *arXiv: 1811.08201 [cs]*.